Hindawi Publishing Corporation
VLSI Design
Volume 2008, Article ID 294014, 10 pages
doi:10.1155/2008/294014

Research Article

Using Signal Envelope Detection for Online and Offline RF MEMS Switch Testing

E. Simeu,[1] H. N. Nguyen,[1] P. Cauvet,[2] S. Mir,[1] L. Rufer,[1] and R. Khereddine[1]

[1] *TIMA Laboratory, 46 Avenue Félix Viallet, 38031 Grenoble Cedex, France*
[2] *NXP Semiconductors, 2 Rue de la Girafe, BP 5120, 14079 Caen Cedex 5, France*

Correspondence should be addressed to E. Simeu, emmanuel.simeu@imag.fr

Received 16 October 2007; Revised 19 February 2008; Accepted 7 April 2008

Recommended by José Machado da Silva

The test of radiofrequency (RF) integrated circuits at their ever-increasing operating frequency range requires sophisticated test equipment and is time-consuming and, therefore, very expensive. This paper introduces a new method combining low-frequency actuation signal as test stimuli and signal envelope detection applied on the RF output signal in order to provide a low-cost mean for production testing of RF MEMS switches embedded in system-in-package (SiP) devices. The proposed approach uses the principle of alternate test that replaces conventional specification-based testing procedures. The basic idea is to extract the high-frequency characteristics of the switch from the signal envelope of the response. Output parameters like "on" and "off" transition time are extracted at low frequency and used in a regression process to predict RF conventional specifications like S-parameters. The paper also provides a set of recursive estimation algorithms suitable for online testing. In this context, "on" and "off" transition time estimated from the output low-frequency envelope is used as test metrics and is concurrently updated using recursive algorithms. Validation results obtained on a capacitive RF switch model are presented.

1. INTRODUCTION

The trend toward more portable solutions, with more embedded functions, drives the demand for the system-in-package (SiP) technology. Cellular handset designs represent a good example of this global trend. Today, a cellular mobile must offer multiband and multimode in addition to Bluetooth networking, global positioning system (GPS), and wireless local area network (WLAN), not to mention the user applications such as games, audio, and video (TV on Mobile). The International Technology Roadmap for Semiconductors defines a system-in-package as any combination of semiconductors, passives, and interconnects integrated into a single package [1]. This definition clearly indicates that an SiP can combine different die technologies and applications with active and passive components to form a complete system or subsystem, whereas a system-on-chip (SoC) is created from one single die. Consequently, an SiP usually includes logic and memory components, but it also increasingly includes analog, mixed-signal and RF components, and micro-electromechanical systems (MEMS). These various components are interconnected by wire-bond, flip-chip, stacked-die technology, or any combination of above. The final packaged SiP is looking like any conventional SoC package. Figure 1 shows an example of interconnection of multiple die components in an SiP for Global system for mobile communication (GSM) application. As shown in Figure 2, different type of carriers can be used to incorporate the whole package made of the dies and their interconnections.

SiP offers a unique advantage over SoC in its ability of integrating MEMS with circuitry to provide a fully functional system, not just acting as a simple sensor or actuator. The need for various RF bands in mobile phones is a key driver for the introduction of components that can switch the received or transmitted RF signal to the appropriate blocks.

These new heterogeneous integrated systems pose many challenges from a test perspective. Generally, because of factors such as cost, quality, and reliability, an SiP must be created from bare dies with a high-quality level, in other terms, from known-good-dies (KGD). The manufacturing process, and particularly the packaging step, is more

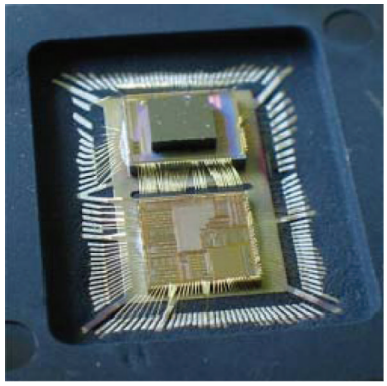

Figure 1: Multiple die components and interconnections on an SiP for GSM application.

complex, potentially increasing the likelihood of failing devices. Indeed, MEMS packaging process is a critical operation on its own because of the requirements for the cavity sealing. Therefore, assembling MEMS into an electronic system puts more requirements on mass production. Last but not least, the test strategy and its consequences on methods and design-for-test (DfT) features must be carefully considered.

In this paper, we aim at developing a low-cost production test approach for RF MEMS switches embedded in SiP devices. Since the RF MEMS switch is embedded together with other devices, the most important difficulty is to obtain measures at the output of the switch in order to detect and diagnose potential faults. In the approach we present, the output of the switch is monitored by means of an envelope detector. The low-frequency output of this detector is then used to predict the actual high-frequency performances of the switch. This approach relaxes the constraints on sampling speed and timing accuracy when applied to very high-speed RF components.

The rest of the paper is structured as follows. First, Section 2 briefly reviews some previous works on RF MEMS testing. Behavioral modeling of capacitive switches is discussed in Section 3. Emphasis is given to dynamic modeling of a series capacitive switch. Section 4 deals with the proposed testing scheme. Different switching parameters are presented and the way of extracting them from the output envelope for offline and online testing purposes is discussed. Monte Carlo simulation and nonlinear regression are discussed in Section 5. The simulation results show accurate prediction of S-parameters using the estimated transient time. Section 6 suggests a set of recursive algorithms for online monitoring of transition times, allowing online testing schemes for RF MEMS switches. Conclusions are given in Section 7.

2. PREVIOUS WORKS

Work on RF integrated circuit testing has been largely triggered by the need of testing RF transceivers. This problem can be illustrated by an example strategy of a path-based testing approach, where a receiver or transmitter channel is tested from antenna to digital baseband as a whole. At a first glance, we might expect that testing the system parameters, such as bit error ratio (BER) for the receiver path or error vector magnitude (EVM) for the transmitter, would ensure a sufficient coverage at a reasonable cost. This is not the case because such a test requires expensive RF instruments, and the test of the RF switch cannot guarantee all the specifications and, more importantly, the quality and the reliability of the component, thus of the whole system.

Because of the long evaluation time needed and expensive RF ATE (automated test equipment) required by elaborate performance tests, the production testing of high performance SiP is a major component of the total manufacturing cost. Indeed, ICs production testers with RF capabilities supporting frequencies of GHz range are prohibitively expensive. Further increase of the costs is due to the key problem with testing RF dies coming from the fact that many complex RF specification values need to be determined during production test at high operating frequencies [2, 3]. Testing a significant number of devices in this way is therefore prohibitive and impractical. RF MEMS switches are among the most test demanding RF devices.

In recent years, alternate tests have been considered as a promising solution for low-cost test of RF components [4–6]. In contrast to the previous work using classical functional testing methods, the test specifications of the device-under-test (DUT) are not measured directly using conventional methods. Instead, in alternate testing approaches, the test specification values of the DUT are computed directly from the observed test response when a specially crafted stimulus is applied.

Previous works on RF MEMS switches [7, 8] have exposed the advantages of testing them at lower test frequency instead of performing the measurements by investigating them at the intended signal frequency. In [7], the reliability assessment of a capacitive shunt switch is considered. It is shown that a low frequency of 10.7 MHz is already sufficient for detecting the main features of the switch cycle such as pull-in voltage, rise- and fall-times of the switching action and the difference between the on-capacitance and the off-capacitance (ΔC). A square wave of 10 kHz is used as actuation signal. The output signal is bandpass filtered around the switched voltage frequency. A diode detector is used for demodulation followed by an amplifier. Although some failure mechanisms may be related to GHz frequencies, it is shown in [7] that many failure modes can be investigated at this lower test frequency. Therefore, the test procedure requires only standard components that are less expensive and easier to use in order to build a measurement sufficiently rich to investigate important properties of the switching behavior, such as rise- and fall-times and stability. Taking the test of an RF MEMS switch as illustration example, in [8] the authors study the monitoring of an SiP integrating MEMS devices. Similarly as in [7], a capacitive shunt switch is used here to illustrate the proposed scheme.

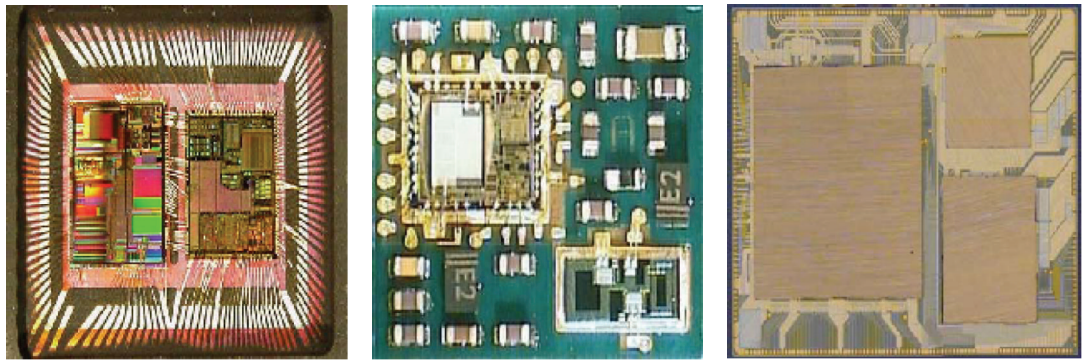

(a) (b) (c)

Figure 2: Examples of carrier style of an SiP package: (a) Leadframe, (b) Laminate, (c) Silicon-Based.

3. BEHAVIORAL MODEL OF CAPACITIVE SWITCHES

A number of different criteria can be used to classify MEMS switches. Taking into account the actuation mechanism, the electrostatic, electromagnetic, or electrothermal principle can be considered. The electrostatic principle is the most convenient for the fabrication that can be compatible with typical RF technologies. Switches based on the electrostatic principle are also smaller and faster.

Depending on the circuit configuration, switches can be of series or parallel (shunt) types. These two configurations are illustrated in Figure 3. The switching element can be designed as a beam fixed on both ends, as a cantilever or as a membrane. The choice of the form of the element is driven by the demand on the switch stiffness that defines the necessary switching voltage or by the facility to be used in certain switch configurations.

The type of switching contacts distinguishes two different approaches to the switch application. There are switches creating a resistive (metal to metal) contact or a capacitive (contact-less) one. The first group allows DC applications and can be used up to 60 GHz, whereas the second group covers the frequency range from 6 to 120 GHz. An important parameter describing the quality of capacitive switches is the capacity ratio in the "on" and "off" states. Typical key specifications of today switches include

(i) $C_{ON}/C_{OFF} > 100$,

(ii) actuation voltage <20 V,

(iii) number of switching cycles to failure $>10^9$,

(iv) $t_{down} \sim 5$ microsecond,

(v) $t_{up} \sim 3$ microsecond.

To allow investigation of phenomena such as pull-down, release, power handling, and source noise effects, a behavioral model of the switch is needed with the control voltage V_c that can be an arbitrary continuous function of time.

3.1. Low-frequency dynamic analysis

There are a number of physical mechanisms available for switch actuation. Among these, the electrostatic (or capacitive) conversion is one of the most mature. This is probably because actuators using this conversion are commonly produced with surface micromachining technology that is compatible with integrated circuit fabrication process.

The electrostatic mechanism is based on the interaction between the mechanical and electrical quantities in a condenser having one electrode fixed and the other electrode movable. A voltage applied between both electrodes causes the displacement of the movable electrode. In a transversal capacitive transducer, the movable electrode is displaced off-plane, perpendicularly to the electrode surface. In order to avoid the electrical contact between actuating electrodes, the dielectric layer between these electrodes must be introduced.

The original distance between the electrodes H defined in Figure 4 varies by the displacement x when the transducer is in function. The instantaneous transducer capacity is

$$C = \frac{\varepsilon A}{H - x + (t_d/\varepsilon_d)}, \tag{1}$$

where $A = Ww$ is the area of electrodes, ε the permittivity of air, t_d and ε_d are the thickness and the relative dielectric constant of the dielectric layer, respectively. Supposing that the voltage does not change during the movement of the movable electrode, the electrostatic force is given by

$$F_e = \frac{\varepsilon A U^2}{2\left(H - x + (t_d/\varepsilon_d)\right)^2}. \tag{2}$$

The dynamic model of the cantilever beam is useful for determining the switching time of the switch, the frequency bandwidth of the mechanical part, and the effect of damping. In case of small displacements, the dynamic response of the MEMS beam is given by

$$m\frac{d^2x}{dt^2} + b\frac{dx}{dt} + kx = \frac{\varepsilon A U^2}{2\left(H - x + (t_d/\varepsilon_d)\right)^2}, \tag{3}$$

where x is the beam displacement, m is the beam mass, the spring constant k due to a uniform force applied over the entire beam is given by

$$k = \frac{2Ew}{3}\left(\frac{T}{a}\right)^3. \tag{4}$$

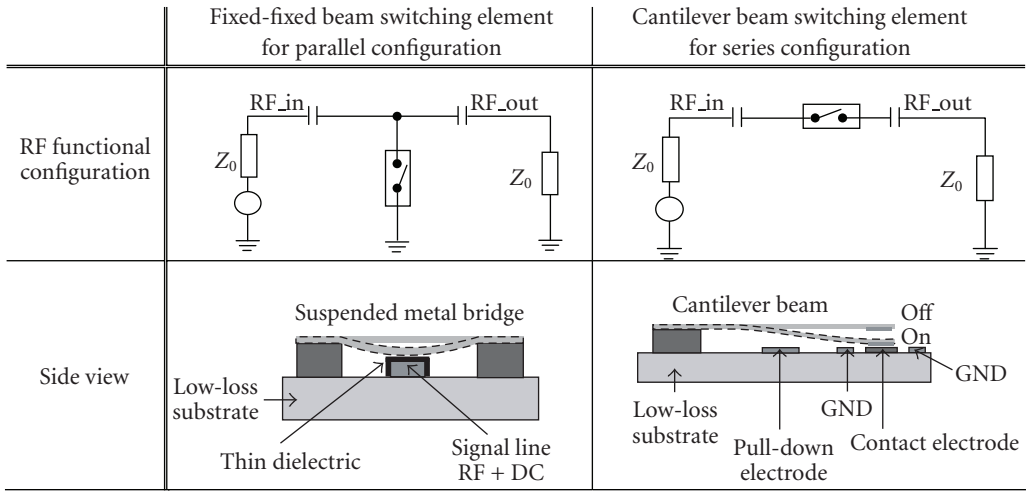

Figure 3: Parallel and series configurations of RF MEMS capacitive switches.

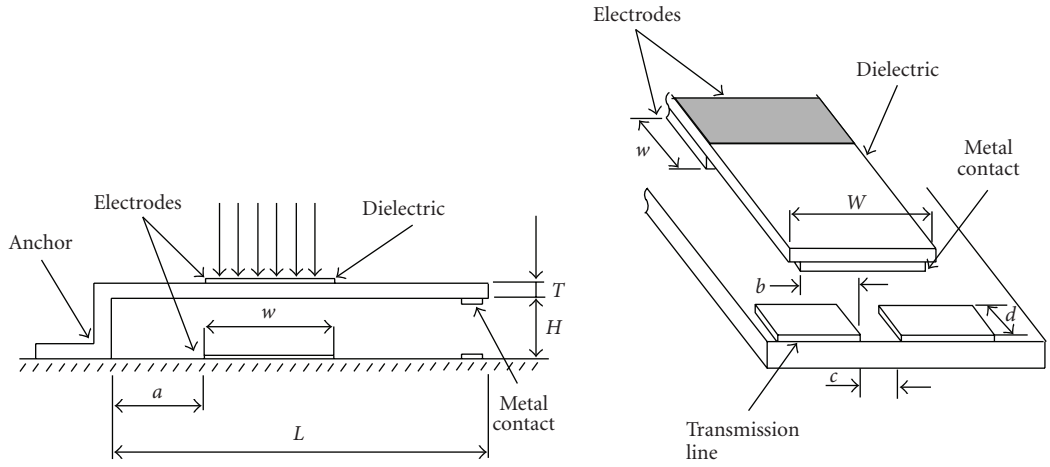

$L = 200\,\mu$m, $W = 50\,\mu$m, $T = 1\,\mu$m, $H = 3\,\mu$m, $w = 100\,\mu$m, $a = 100\,\mu$m, $b = 15\,\mu$m, $c = 10\,\mu$m, $d = 20\,\mu$m

(c)

Figure 4: Design parameter of a cantilever beam switch: (a) side view and (b) perspective view.

An approximate formula for the damping coefficient for a cantilever beam is given in [9] by

$$b = \frac{3\mu S^2}{2\pi H^3}, \tag{5}$$

where S is the area of the beam, a, T, H, and w are the design parameters defined in Figure 4, and E and μ are Young's modulus and the coefficient of viscosity, respectively.

3.2. High-frequency equivalent circuit

A capacitive series switch with resistive (metal-to-metal) contact is shown in Figure 5(a). The corresponding circuit model of the RF section is shown in Figure 5(b). For a cantilever switch with two contact areas, the capacitance is composed of a series capacitance (C_s) between the transmission lines and the switch metal and a parasitic capacitance (C_p) between the open ends of the transmission lines. The total series capacitance is $C_s/2$ with

$$C_s = \frac{\varepsilon A_s}{H - x + (t_d/\varepsilon_d)}, \tag{6}$$

where A_s is the contact area in both sides. It is seen that the capacitance C_s has a strong dependence on the displacement x. The MEMS series switch resistance between the contact areas is dependent on its length and width. The transmission line loss must be added to obtain the total switch resistance which is assumed constant. In the down-state position, it is possible to model the transmission lines by a series inductance. For simplicity, the inductance of the switch is supposed negligible in the rest of the paper and the

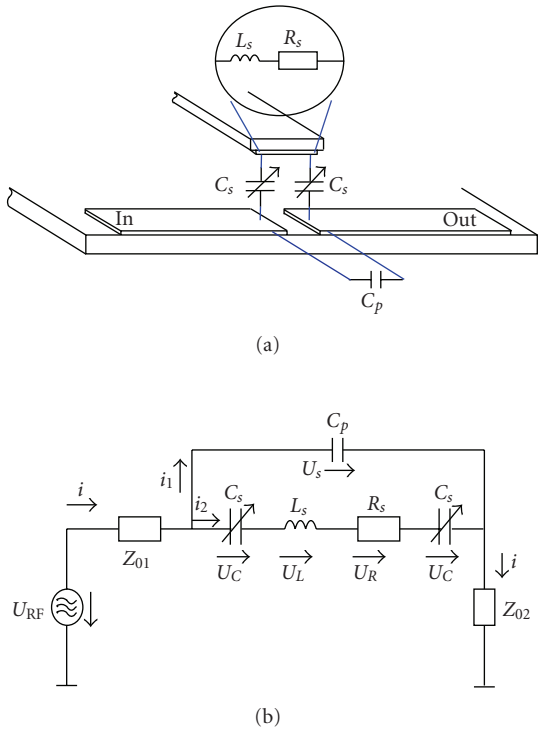

FIGURE 5: (a) RF capacitive switch showing the input and output RF transmission line and the switching contact placed on the free end of the cantilever, and (b) circuit model corresponding to the RF behavior.

impedances Z_{01} and Z_{02} represent incoming and outgoing transmission line sections.

3.3. *Complete model of the switch*

The equations governing the complete behavior of the switch can be readily solved with a nonlinear simultaneous differential equation solver such as Matlab/Simulink. The complete model of the series switch is given in Figure 6. For the simulation of this model, the physical parameter values given in Figure 4 have been considered.

4. USING ENVELOPE DETECTION TO EXTRACT LOW-FREQUENCY OUTPUT PARAMETERS

In order to facilitate the embedded test of an RF switch, the evaluation of the test response needs to be handled by an on-chip analog detector with a low-frequency output. In this work, we use an embedded envelope detector to capture a low-frequency signal describing the switching behavior of the device. Figure 7 shows an envelope detector embedded in an RF MEMS serial switch. It consists simply of a diode and resistor-capacitor (RC) filter.

In a positive half cycle of the input signal, the diode is forward biased and the capacitor C_t charges up rapidly to a peak value of the input signal. When the input signal falls below this value, the diode becomes reverse biased and the capacitor discharges slowly through the load resistor R_t. The discharging process continues until the next positive half cycle. Thereafter the charging-discharging cycle is continued. The values of R_t and C_t are to be chosen appropriately to perform the required envelope detection. The envelope detector output signal is shown in Figure 8.

An RF input signal of 1 GHz is applied to the incoming transmission line of the switch and a simple pulse signal (Figure 8(a)) is applied to its electrodes as actuation input. The RF output signal obtained on the outgoing transmission line is plotted in Figure 8(b). The corresponding envelope detector output is represented in Figure 8(c).

For an actuation signal applied to the switch (functional, or a special test actuation), easily measurable output parameters must be extracted from the observed low-frequency test response. Conventional performances (such as *S*-parameters) can be predicted from this estimation using a nonlinear regression equation. The following output parameters can be extracted from the low-frequency test response.

(i) Transition time. This is given by the time to switch from the "off" to the "on" state and vice versa. The conventional definition of the transition times is the time required for the output RF signal to rise from 10% to 90% of its value for off-to-on transition and 90% to 10% for on-to-off transition. However, since the corresponding values will be difficult to evaluate, we will use the definition of t_{on} and t_{off} given in Figure 9. These values are easily obtained from the output envelope as shown in Figure 9.

(ii) Off/on voltage ratio. This parameter is given by the ratio of the test signal amplitudes in the "off" and "on" states. A good approximation of this ratio is given by A_{off}/A_{on}, where A_{on} and A_{off} are, respectively, the switch on- and the switch off- envelope amplitudes defined in Figure 9.

(iii) Actuation voltages. The switch-on voltage V_{on} is the minimal voltage required to switch the device from the "off" to the "on" state. The switch-off voltage V_{off} has an analog definition.

5. COMPUTING S-PARAMETERS FROM LOW-FREQUENCY OUTPUT PARAMETERS

Monte Carlo simulation was combined with a nonlinear regression analysis to generate mappings from the low-frequency output parameters to high-frequency *S*-parameters. A Monte Carlo simulation is first done to generate a sample of 200 switches. A Gaussian distribution is applied for each physical parameter given in Figure 6, with a variation coefficient of 0.4 (standard deviation = 0.4 × nominal value).

For each of the 200 switches, the *S*-parameters are computed at an operating frequency of 1 GHz. The alternate test stimulus is a simple low-frequency pulse signal. The feature extraction algorithm uses the signal envelope to compute an estimation of the transition time (T_{on} and T_{off}). These samples are fed into a regression model generated

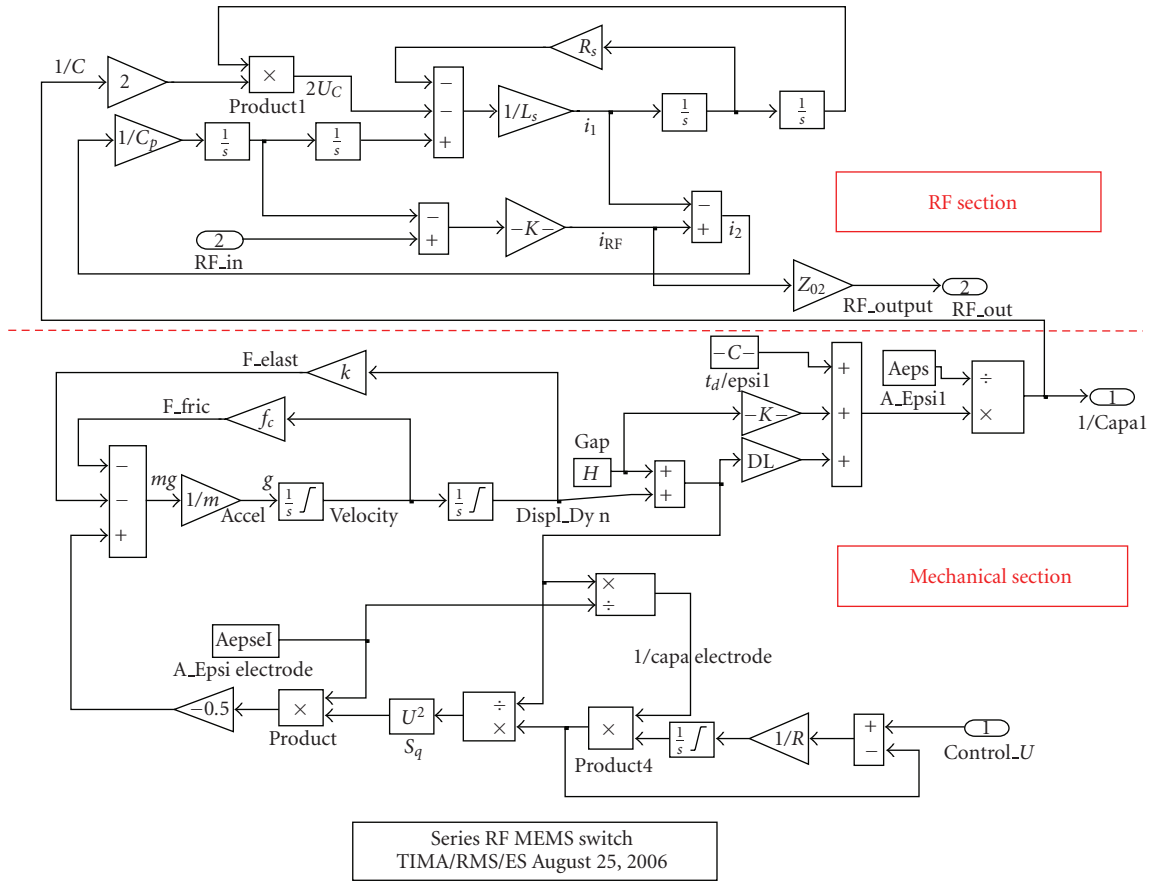

Figure 6: Matlab/Simulink dynamic model of the RF switch.

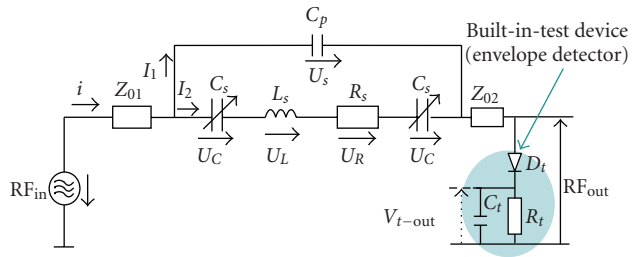

Figure 7: Envelope detector embedded in an RF MEMS serial switch scheme.

by 100 instances of the switch Matlab/Simulink model. The regression procedure aims at finding the best fitting curve to the set of 100 points by minimizing size of the offsets (the residuals) of the points from the curve. The least square regression methods use the sum of the squares of the offsets instead of the offset absolute values because this allows the residuals to be treated as a continuous differentiable quantity. Our experimental procedure aims at providing a fitting function for the independent variable X which is a vector of component T_{on} and T_{off} that estimates high-frequency parameter S_{ij} for a given $x = (t_{\text{on}}, t_{\text{off}})$. The linear least squares fitting technique is the simplest and the most commonly used form of regression method that provides a much simpler analytic form for the fitting parameters than other nonlinear regression fitting algorithm such as MARS [10] which is used in [4, 5, 11] for alternate test. In addition, the fitting technique can be easily generalized from a linear fitting to any nonlinear expression provided that the parameters to be estimated appear linearly in the fitting function. In fact, the functional relationship between the S_{ij} and $x = (t_{\text{on}}, t_{\text{off}})$ is assumed to be a combination of nonlinear expressions as exponential (e^x), power (x^n), and logarithm (lnx), with additive or multiplicative constants. The data are first transformed in such a way that the resulting line is a straight line. For this reason, standard forms for exponential, logarithmic, or power laws in the nonlinear fitting function expression are first explicitly computed.

The accuracy of the regression result is validated by a separate set of 100 instances that are generated independently from the training set. Figure 10 shows the predicted versus actual specifications of 100 instances in this validation set for S_{12} and S_{12} specification parameters. As shown in Figure 10, the specification S_{12} is predicted with a relatively good accuracy using only the transition times.

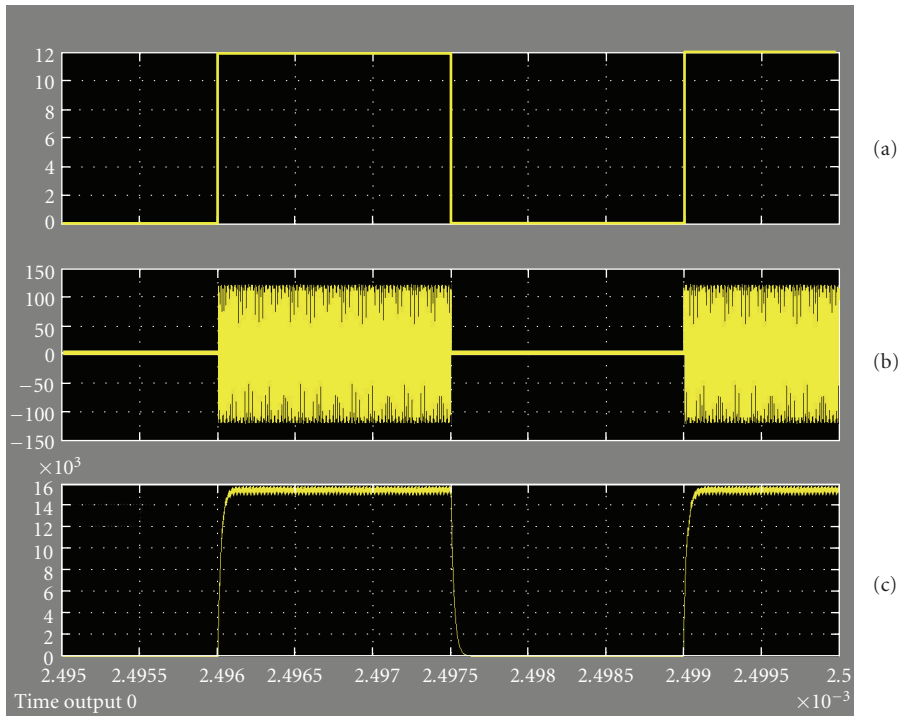

Figure 8: Test signal simulation: (a) switch actuation control signal, (b) RF output signal, (c) detected envelope of the output signal.

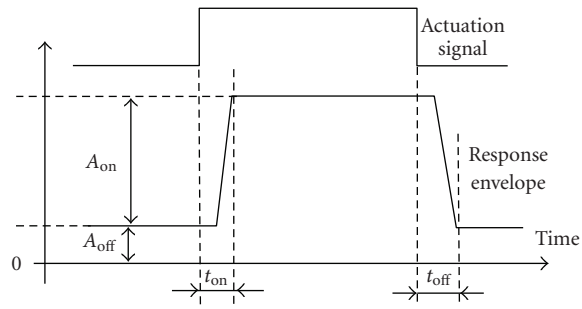

Figure 9: Low-frequency output parameters: t_{on} is the total delay time of a rising edge; t_{off} is the total delay time of a falling edge; A_{on} is the envelope amplitude in the "on" state; and A_{off} is the envelope amplitude in the "off" state.

6. RECURSIVE ESTIMATION-BASED ONLINE MONITORING OF TRANSITION TIMES

In this section, we are suggesting three recursive estimation algorithms that can be used for online monitoring of low-frequency test metrics extracted from the switching envelope signal. All the switching characteristics can be used as test metrics in a procedure of low-frequency offline testing as well as in online monitoring scheme. In the offline testing case, a special test stimulus is applied on the actuation input of the switch. The test decision is taken by comparing the switching characteristics estimated from the output envelope to their nominal values. In the context of online testing scheme, the switching characteristics are estimated concurrently to the normal operation of the switch by means of a recursive identification algorithm. The value of each of the test metrics is updated at each operation. For the switching cycle K, an estimation $\hat{\theta}(t)$ of the mean value of the switching test metric $\theta(t)$ is given by

$$\hat{\theta}(t) = \frac{1}{t}\sum_{i=1}^{t}\varphi(i), \tag{7}$$

where $\hat{\theta}(t)$ is the mean value of the parameter for the t first switching cycles and φ(i) is the value of the test metric measured for the switching cycle i. Since new data appears recursively, we must avoid repeating all calculations at each stage. This involves the use of a recursive formula that expresses $\hat{\theta}(t)$ in terms of $\hat{\theta}(t-1)$.

Theorem 1. *A recursive form of* (7) *expressing* $\hat{\theta}(t)$ *in terms of* $\hat{\theta}(t-1)$ *is (see proof in the appendix)*

$$\hat{\theta}(t) = \frac{t-1}{t}\hat{\theta}(t-1) + \frac{\phi(t)}{t}. \tag{8}$$

In the context of online testing, it is necessary to adapt the estimator quickly when appears a change in the device. Weighting factors are introduced in the mean value calculation to give more weight to the new data compared

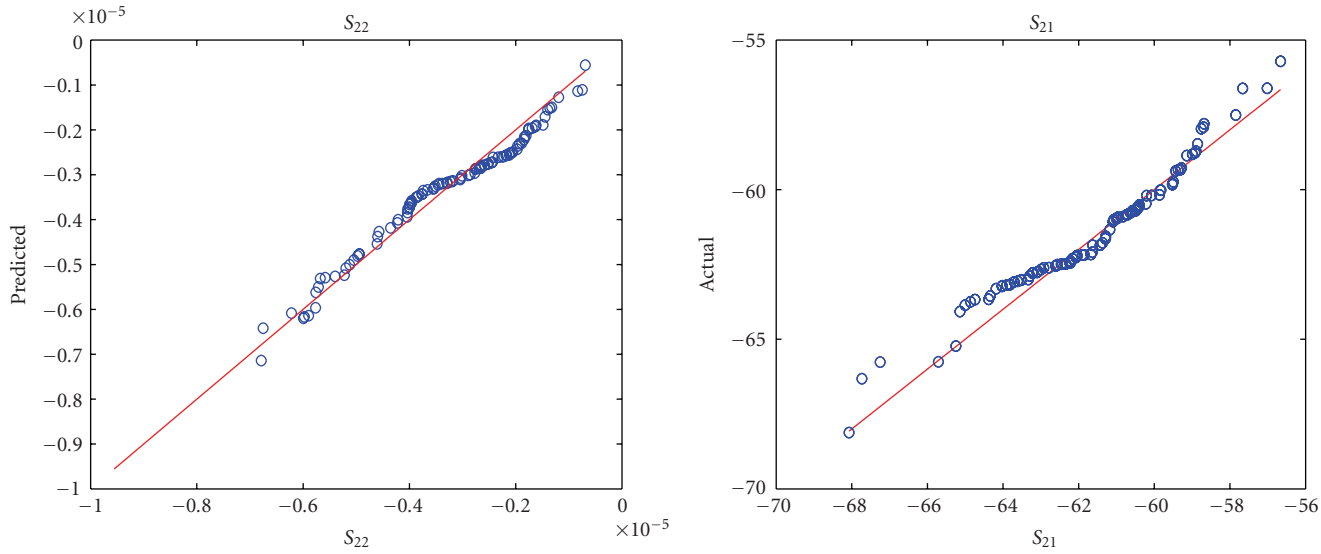

Figure 10: Predicted S-parameter for RF MEMS Switch.

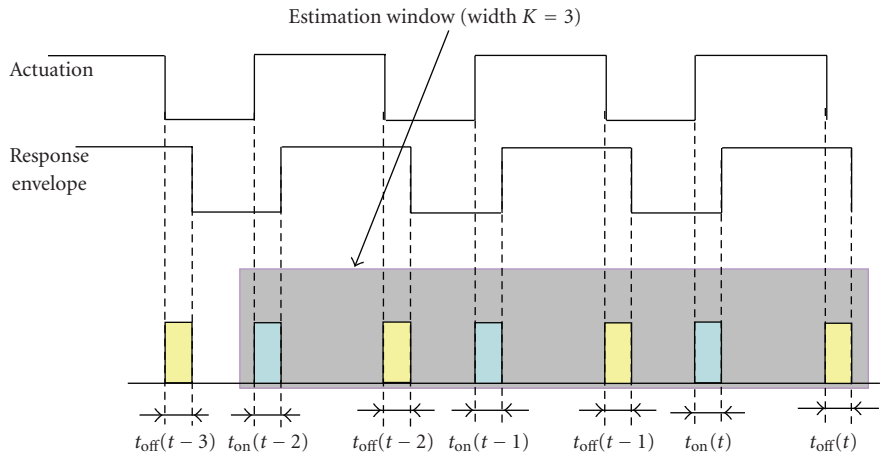

Figure 11: Sliding window recursive estimation.

with the older. The weighting or forgetting factors allow then to forget old information. The mean value is then given by

$$\hat{\theta}_\lambda(t) = \frac{\lambda^t\phi(0)+\lambda^{t-1}\phi(1)+\cdots+\lambda^{t-i}\phi(i)+\cdots+\lambda\phi(t)+\phi(t)}{\lambda^t+\lambda^{t-1}+\cdots+\lambda^{t-i}+\cdots+\lambda+1} = \frac{\sum_{i=0}^{t}\lambda^{t-i}\phi(i)}{\sum_{i=0}^{t}\lambda^i}, \tag{9}$$

where the forgetting factor λ verifies: $0 < \lambda < 1$.

Theorem 2. *When the time value t is great enough, a recursive form of* (9) *expressing* $\hat{\theta}_\lambda(t)$ *in terms of* $\hat{\theta}_\lambda(t-1)$ *is given by (see proof in the appendix)*

$$\hat{\theta}_\lambda(t) = \lambda\hat{\theta}_\lambda(t-1) + (1-\lambda)\phi(t). \tag{10}$$

In another recursive estimation algorithm, only the data included in a sliding window are used in the estimation formula. All the past data that are out of this sliding window are not taken in the updating of the test metric estimation value. The mean value of the test metric is then estimated through a sliding window of width K as shown in Figure 11 (for $K = 3$).

In this case, the mean value estimation is given by the following definition equation:

$$\hat{\theta}_K(t) = \frac{1}{K}\sum_{i=0}^{K-1}\phi(t-i), \tag{11}$$

where K is the width of the estimation window.

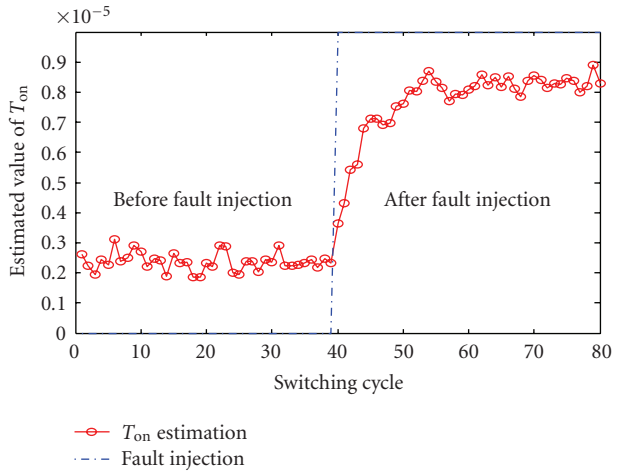

FIGURE 12: Simulation of recursive estimation for online fault detection using the sliding window algorithm.

Theorem 3. *A recursive form of* (11) *expressing* $\hat{\theta}_K(t)$ *in terms of* $\hat{\theta}_K(t-1)$ *is given by (see proof in the appendix)*

$$\hat{\theta}_K(t) = \hat{\theta}_K(t-1) + \frac{\phi(t) - \phi(t-K)}{K}. \tag{12}$$

To test the efficiency of the proposed online testing scheme, many fault injections have been simulated on the RF MEMS switch Matlab/Simulink model of Figure 5. Among the recursive algorithms proposed above, the sliding window method seems to be a good trade-off between the complexity of online fault detection scheme and its efficiency in terms of fault latency and fault coverage.

Figure 12 gives an example of parametric fault detection using the estimation of off-to-on transition time. A parametric fault corresponding to a 50% decrease of the electrode area ($A = Ww$) was injected in the behavioral model of the switch. It is evident that this is a typical parametric manufacturing fault. However, this type of fault may also occur in an operating application when the hermetic packaging requirements of RF MEMS switch are no longer guaranteed. It is clear from this figure that the injected fault is quickly detected since the T_{on} mean value estimated before the fault injection is soon significantly different than the mean value obtained after the fault injection.

7. CONCLUSIONS

The main objective of this work is to find a way of testing RF MEMS switches that leads to a low-cost implementation and that speeds up the whole process of conventional functional testing of RF devices embedded in SiP packages. We have suggested a testing scheme of capacitive RF MEMS switches based on an envelope detector that provides a low-frequency output. Simulation results show that this signal provides important properties of the switching behavior, such as transition times, actuation voltage, and switching voltage ratio. From data provided by Monte Carlo simulation, we have implemented a multivariate regression algorithm to build nonlinear mappings that link the low-frequency test metrics to conventional specifications parameters of RF devices such as *S*-parameters that are available at RF operating frequency only. As a consequence, the conventional high-frequency specifications of the switch are predictable from the low-frequency signal envelope. The results obtained using the proposed methodology show that the high-frequency specifications can be predicted with good accuracy from the transition time measurement. In the proposed methodology, the test is performed using a low-frequency envelope signal without requiring access to high-frequency information, thus eliminating the need for expensive RF ATE. For online testing purposes, the paper also provides a set of recursive algorithms aiming at low-cost online monitoring of low-frequency test features extracted from the switching envelope signal, instead of testing the RF device at its typical operating frequency.

APPENDIX

Proof of Theorem 1. The mean value estimation of the test metric $\theta(t)$ for the t first measurements is given by

$$\hat{\theta}(t) = \frac{1}{t}\sum_{i=1}^{t}\varphi(i) \;= \frac{1}{t}\sum_{i=1}^{t-1}\varphi(i) + \frac{1}{t}\varphi(t)\ ,$$

Since

$$\frac{1}{t}\sum_{i=1}^{t-1}\varphi(i) = \frac{t-1}{t}\left(\frac{1}{t-1}\sum_{i=1}^{t-1}\varphi(i)\right) = \frac{t-1}{t}\theta(t-1),$$

$$\hat{\theta}(t) = \frac{1}{t}\sum_{i=1}^{t-1}\varphi(i) + \frac{1}{t}\varphi(t) = \frac{t-1}{t}\hat{\theta}(t-1) + \frac{\varphi(t)}{t}. \tag{A.1}$$

□

Proof of Theorem 2. Since the weighted mean value estimation of the test metric is given by

$$\hat{\theta}_\lambda(t) = \frac{\sum_{i=0}^{t}\lambda^{t-i}\varphi(i)}{\sum_{i=0}^{t}\lambda^{i}} = \frac{N_\lambda(t)}{D_\lambda(t)} \tag{A.2}$$

for the numerator term we have

$$\begin{aligned} N_\lambda(t) &= \sum_{i=0}^{t}\lambda^{t-i}\varphi(i) \\ &= \sum_{i=0}^{t-1}\lambda^{t-i}\varphi(i) + \varphi(t) \\ &= \lambda\left(\sum_{i=0}^{t-1}\lambda^{(t-1)-i}\varphi(i)\right) + \varphi(t) \\ &= \lambda\cdot N_\lambda(t-1) + \varphi(t). \end{aligned} \tag{A.3}$$

And for the denominator $D_\lambda(t)$ we have

$$D_\lambda(t) = \sum_{i=0}^{t}\lambda^i = 1 + \lambda\sum_{i=0}^{t-1}\lambda^i = 1 + \lambda\left(\sum_{i=0}^{t}\lambda^i - \lambda^t\right) = 1 - \lambda(D_\lambda(t) - \lambda^t). \tag{A.4}$$

Then $D_\lambda(t) = (1-\lambda^{t+1})/(1-\lambda)$ and finally it follows that

$$\hat{\theta}_\lambda(t) = \frac{N_\lambda(t)}{D_\lambda(t)} = \frac{\lambda\cdot N_\lambda(t-1)}{(1-\lambda^{t+1})/(1-\lambda)} + \frac{\varphi(t)}{(1-\lambda^{t+1})/(1-\lambda)}, \tag{A.5}$$

and since $D_\lambda(t-1) = (1-\lambda^t)/(1-\lambda)$ we have

$$\hat{\theta}(t) = \frac{\lambda.}{(1-\lambda^{t+1})/(1-\lambda)}\frac{1-\lambda^t}{1-\lambda}\frac{N_\lambda(t-1)}{D_\lambda(t-1)} + \frac{\varphi(t)}{(1-\lambda^{t+1})/(1-\lambda)} = \frac{(1-\lambda^t)\lambda\hat{\theta}_\lambda(t-1) + (1-\lambda)\varphi(t)}{1-\lambda^{t+1}}, \tag{A.6}$$

and finally for t great enough since $0 < \lambda < 1$, $\lambda^t \underset{t\to\infty}{\to} 0$, it follows that

$$\hat{\theta}_\lambda(t) = \frac{(1-\lambda^t)\lambda\hat{\theta}_\lambda(t-1) + (1-\lambda)\varphi(t)}{1-\lambda^{t+1}} \underset{t\to\infty}{\longrightarrow} \lambda\hat{\theta}_\lambda(t-1) + (1-\lambda)\varphi(t). \tag{A.7}$$

□

Proof of Theorem 3. For an estimation window width K, the mean value estimation of the test metric is given by

$$\hat{\theta}_K(t) = \frac{1}{K}\sum_{i=0}^{K-1}\varphi(t-i) = \frac{1}{K}\left[\left(\sum_{i=0}^{K-1}\varphi(t-i) - \varphi(t) + \varphi(t-K)\right) + \varphi(t) - \varphi(t-K)\right],$$

$$\hat{\theta}_K(t) = \frac{1}{K}\left[\left(\sum_{i=0}^{K-1}\varphi((t-1)-i)\right) + \varphi(t) - \varphi(t-K)\right].$$

Then $\hat{\theta}_K(t) = \hat{\theta}_K(t-1) + \dfrac{\varphi(t)-\varphi(t-K)}{K}$. (A.8)

□

REFERENCES

[1] SIA, "Assembly and packaging," *The International Technology Roadmap for Semiconductors*, Semiconductor Industry Association, San Jose, Calif, USA, 2005.

[2] T. Wilson, "Test challenges of next-generation RF digital devices," *EE: Evaluation Engineering*, vol. 39, no. 11, pp. 31–37, 2000.

[3] M. S. Huetmaker, "RF/analog test of circuits and systems," in *Proceedings of the 18th IEEE VLSI Test Symposium (VTS '00)*, pp. 179–182, Montreal, Canada, April-May 2000.

[4] S. Akbay and A. Chatterjee, "Built-in test of RF components using mapped feature extraction sensors," in *Proceedings of the 23rd IEEE VLSI Test Symposium (VTS '2005)*, pp. 243–248, Palm Springs, Calif, USA, May 2005.

[5] B. Kim, H. Shin, J. H. Chun, and J. A. Abraham, "Predicting mixed-signal specifications with improved accuracy using optimized signatures," in *Proceedings of the 11th IEEE Annual International Mixed-Signals Testing Workshop (IMSTW '05)*, Cannes, France, June 2005.

[6] P. N. Variyam and A. Chatterjee, "Enhancing test effectiveness for analog circuits using synthesized measurements," in *Proceedings of the 16th IEEE VLSI Test Symposium (VTS '98)*, pp. 132–137, Monterey, Calif, USA, April 1998.

[7] W. M. van Spengen, R. Puers, R. Mertens, and I. De Wolf, "A low frequency electrical test set-up for the reliability assessment of capacitive RF MEMS switches," *Journal of Micromechanics and Microengineering*, vol. 13, no. 5, pp. 604–612, 2003.

[8] N. Dumas and A. Richardson, "Towards a health monitor for system in package with MEMS functionality," in *Proceedings of the 12th IEEE Annual International Mixed-Signals Testing Workshop (IMSTW '06)*, pp. 151–156, Edinburgh, UK, June 2006.

[9] G. M. Rebeiz, *RF MEMS: Theory, Design and Technology*, John Wiley & Sons, New York, NY, USA, 2003.

[10] J. H. Friedman, "Multivariate adaptive regression splines," *The Annals of Statistics*, vol. 19, no. 1, pp. 1–67, 1991.

[11] R. Voorakaranam and A. Chatterjee, "Test generation for accurate prediction of analog specifications," in *Proceedings of the 18th IEEE VLSI Test Symposium (VTS '00)*, pp. 137–142, Montreal, Canada, April-May 2000.